 ©2007 Kvantovaya Elektronika and Turpion Ltd

PACS numbers: 42.55.Px; 42.60.Da; 42.60.Mi
DOI: 10.1070/QE2007v037n06ABEH013460

Conditions for two-frequency lasing in coupled-cavity vertical-cavity surface-emitting lasers

A.S. Logginov, A.G. Rzhanov, D.V. Skorov

***Abstract*. A self-consistent model of a semiconductor coupled-cavity vertical-cavity surface-emitting laser is presented. The electromagnetic field distribution in the laser is found by the effective-frequency method. The dynamic model is constructed on coupled rate equations for two active cavities. Dynamic, threshold and spectral parameters of the laser are studied. The applicability of the model is confirmed by the good agreement with the experimental data available in the literature.**

Keywords: *semiconductor lasers, vertical-cavity surface-emitting lasers, two-frequency lasers, mathematic simulation.*

1. Introduction

A vertical-cavity surface-emitting laser (VCSEL) is one of the simplest and efficient sources of optical radiation [1]. The advantages of these lasers are the possibility of obtaining the axially symmetric radiation patterns, low threshold currents, and single-longitudinal mode lasing. VCSELs have already gained wide applications in optoelectronics and replaced in a number of cases end-emitting semiconductor lasers. A number of works have recently appeared in which a novel type of VCSELs – coupled-cavity vertical-cavity surface-emitting lasers (CC-VCSELs) is considered [2 – 7].

The studies of conventional semiconductor lasers with several combined cavities have revealed a number of interesting features of these lasers. Thus, cleaved coupled-cavity lasers (C^3 lasers) have been successively used for wavelength tuning while preserving the single-mode regime [8]. However, C^3 lasers are complex in design, the control of coupling between cavities is complicated, the radiation pattern is asymmetric and the wavelength tuning is discrete. Recent experiments [2] have demonstrated the possibility to combine the advantages of VCSELs and C^3 lasers. Unlike C^3 lasers, in CC-VCSELs several cavities are formed without cleaving or etching facets of a semiconductor crystal. The second cavity can be grown on the first cavity directly behind the middle Bragg mirror whose transmission coefficient determines coupling between the cavities. Thus, such a two-frequency radiation source consists of three Bragg mirrors forming two cavities, the excitation level of each of the cavity being controlled separately (Fig. 1).

Coupled-cavity surface-emitting lasers have important features for practical applications. They can provide high-power single-transverse mode lasing [3], control of radiation polarisation [4], and efficient pumping of the second cavity by radiation from the first cavity [5]. Taking into account the fact that active layers in the additional cavity can be considered as saturable absorbers, we can assume the presence of self-modulation and optical instability regimes in CC-VCSELs. The latter regime has been already observed in experiments [6]. On the other hand, one of the most promising applications of this laser is its use as a two-frequency radiation source [2].

Two-frequency lasers can be used in devices for data reading and writing, in dense wavelength-division multiplexing communication systems, in ranging interferometry and in optical gyroscopes. Traditionally, either two combined semiconductor lasers or gas lasers are used for these purposes. Such radiation sources are rather bulky, complex in design and expensive. A more convenient solution of the above-mentions problems is the use of CC-VCSELs.

A detailed theoretical study of CC-VCSEL properties, on the one hand, is necessary for the optimal construction of such devices, and on the other hand, will allow one to determine all the practical possibilities of these devices. At present, one can find in the literature only examples of self-consistent VCSEL models with one cavity [9]. There is also paper [7] considering simplified (neglecting spatial coordinates) rate equations for CC-VCSELs, which do not take into account the optical parameters of the laser. In this paper we present a self-consistent electrooptical model of a CC-VCSEL void of the above disadvantages and numerically analyse dynamic parameters of these lasers.

2. The model

2.1 The wave equation

We will study the optical field distribution inside the CC-VCSEL by using the efficient-frequency method [10 – 12], whose high accuracy in investigations of VCSELs was confirmed in [12] by comparing different simulation methods. In this paper we consider the axially symmetric CC-VCSEL, however the model takes into account the peculiarities of structures without the axial symmetry, unlike the above approaches.

A.S. Logginov, A.G. Rzhanov, D.V. Skorov Department of Physics, M.V. Lomonosov Moscow State University, Vorob'evy gory, 119992 Moscow, Russia; e-mail: sdv_main@mail.ru

Received 19 October 2006
Kvantovaya Elektronika **37** (6) 534 – 540 (2007)
Translated by I.A. Ulitkin

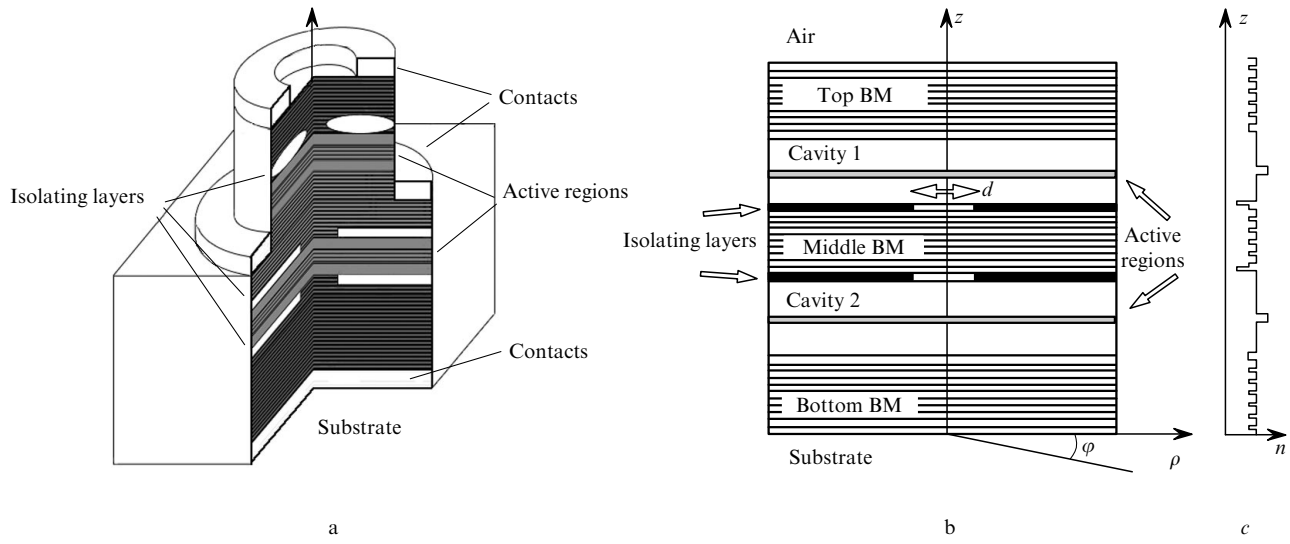

Figure 1. Design of the CC-VCSEL: three-dimensional view (a), sectional view (b), refractive index profile n along the z axis (c); BM is the Bragg mirror and d is the diameter of the isolating aperture.

The main idea of the method consists in the representation of a three-dimensional scalar Helmholtz equation by two equations, which describe the radiation propagation in directions perpendicular to the mirrors (along the z axis) and in the plane of laser layers, where the polar coordinates ρ and φ are specified, as shown in Fig. 1.

Consider the scalar Helmholtz equation, in which the product $\omega^2 n^2(\boldsymbol{r},\omega)/c^2$ was expanded into a series near the frequency ω_0 to the second term inclusive:

$$\left[\Delta + k_0^2 n^2(\boldsymbol{r})\right] E(\boldsymbol{r}) = v k_0^2 n(\boldsymbol{r}) n_g(\boldsymbol{r}) E(\boldsymbol{r}), \tag{1}$$

where ω_0 is the Bragg frequency of the laser mirrors; $\boldsymbol{r}$ is the radius vector; c is the speed of light in vacuum. Here the parameter $v = 2(\omega_0 - \omega)/\omega = 2(\lambda - \lambda_0)/\lambda_0 - 2\mathrm{i}(\mathrm{Im}\,\omega)/\omega_0$ is introduced, which plays the role of the eigenvalue in equation (1). Its real part characterises the frequency detuning, while the imaginary part determines the Q factor of the corresponding mode. $k_0 = \omega_0/c$ is the wave number in vacuum, and $n(\boldsymbol{r})$ and $n_g(\boldsymbol{r})$ are the phase and group refractive indices, respectively.

By separating the variables, we represent the electromagnetic field distribution as a product of functions depending on different coordinates:

$$E(\boldsymbol{r}) = f(z,\rho,\varphi)\Phi(\rho,\varphi). \tag{2}$$

In this case, equation (1) splits into two equations, which form the basis of problems for eigenvalues and eigenfunctions for longitudinal and transverse laser modes:

$$\left[\frac{\mathrm{d}}{\mathrm{d}z^2} + k_0^2 n^2(\boldsymbol{r})\right] f(z,\rho,\varphi) = v_{\mathrm{eff}} k_0^2 n(\boldsymbol{r}) n_g(\boldsymbol{r}) f(z,\rho,\varphi), \tag{3}$$

$$\left[\frac{\Delta_{\rho,\varphi}}{k_0^2 \langle n n_g\rangle} + v_{\mathrm{eff}}(\rho,\varphi)\right] \Phi(\rho,\varphi) = v\Phi(\rho,\varphi). \tag{4}$$

The average product of the phase and group refractive indices over the length of the composite CC-VCSEL cavity

$$\langle n n_g\rangle = \int_0^{L_{\mathrm{cav}}} n(\boldsymbol{r}) n_g(\boldsymbol{r}) f(z,\rho,\varphi)\mathrm{d}z$$

is the function of ρ, φ. We calculated this value by assuming that the function $f(z,\rho,\varphi)$ is normalised as

$$\int_0^{L_{\mathrm{cav}}} |f(z,\rho,\varphi)|^2 \mathrm{d}z = 1,$$

and introducing the notation $v_{\mathrm{eff}}(\rho,\varphi)$, which represents a set of eigenvalues of equation (3) for different points with coordinates ρ, φ. A coupled-cavity surface-emitting laser is considered as a unified device in which, unlike a conventional VCSEL, two longitudinal modes falling into the active-medium gain profile are excited. Therefore, two sets of eigenvalues will correspond to equation (3) for each point with coordinates ρ, φ, and own solutions of Eqn (4) will correspond to each of these sets.

The sequence of calculations according to this method for each longitudinal mode is as follows:

(i) The problem of eigenvalues and eigenfunctions (3) for all points with coordinates ρ, φ is solved.

(ii) The functions $\langle n n_g\rangle$ и $v_{\mathrm{eff}}(\rho,\varphi)$ are calculated from the obtained solutions.

(iii) The problem of eigenvalues and eigenfunctions (4) with the obtained functions as parameters is solved.

(iv) The radiation intensity distribution in the laser is constructed according to (2).

A detailed substantiation of the effective-frequency method can be found in [10].

2.2 Parameters of the active region

(i) Let us assume that the injection current in the CC-VCSEL is concentrated in the region confined by the nonconducting oxide apertures (isolating layers in Fig. 1) and spreads around on the way to the active region. This process can be approximated by the function [13]

$$J(\rho,\varphi) = \exp\left[-(\rho/R_{\mathrm{act}})^6\right] \exp\left[m(\rho/R_{\mathrm{act}})^2\right],$$

where $J(\rho,\varphi)$ is the injection current density; m is the parameter determined by the contact geometry; $R_{\rm act}$ is the radius of the isolating aperture. This assumption is based on the fact that the distance between the isolating apertures and active layers in VCSELs is usually small, about of 100 nm, and hence, the radius of the region of the current spread is determined mainly by the radius of the isolating layers [9].

(ii) The dependence of the refractive index of active layers on the carrier concentration N is assumed linear [9]:

$$n(\rho,\varphi) = n_0(\rho,\varphi) + \frac{{\rm d}n}{{\rm d}N}N(\rho,\varphi),$$

where $n_0(\rho,\varphi)$ is the refractive index of the matter for the zero concentration of redundant carriers; ${\rm d}n/{\rm d}N$ is the nonlinear refraction coefficient characterising the matter in the active medium.

(iii) We will use the linear dependence of the active medium gain on the carrier concentraction:

$$g = g_0(N - N_{\rm trans}), \tag{5}$$

where g_0 is the gain depending on the radiation frequency and material properties; and $N_{\rm trans}$ is the current carrier concentration, which corresponds to the transparency threshold of the active-layer medium.

2.3 Rate equations

The general form of rate equations for a CC-VCSEL is similar to that for other semiconductor lasers. However, while considering CC-VCSELs, it is necessary to take into account the presence of two active regions localised in different cavities and coupling between them. We will denote the generated modes by indices S and L corresponding to the shorter and longer wavelengths, respectively. The interaction between the cavities consists in the following:

(i) when the gain exceeds the threshold in both active regions, the longitudinal L and S modes cause recombination of carriers and, hence, are amplified in both cavities;

(ii) if one of the active regions is pumped below the transparency level, it absorbs photons resonantly in both longitudinal modes. As a result, the carrier concentration can increase in the active region under study, i.e. the optical pumping of the passive cavity is realised;

(iii) photons produced in spontaneous recombination fall into both longitudinal modes.

These features are described by the rate equations for two active regions of the CC-VCSEL:

$$\frac{\partial N_i}{\partial t} = \frac{J_i}{ed_i} - \frac{N_i}{\tau_{\rm sp}} + D_i\Delta_{\rho,\varphi}N_i - \frac{C}{n_{{\rm g}\,i}}\Gamma_i^{\rm S}g_i(N_i,\lambda^{\rm S})\sum_j S^{{\rm S},j}|\Phi^{{\rm S},j}|^2$$

$$- \frac{c}{n_{{\rm g}\,i}}\Gamma_i^{\rm L}g_i(N_i,\lambda^{\rm L})\sum_j S^{{\rm L},j}|\Phi^{{\rm L},j}|^2, \tag{6}$$

where $i = 1, 2$; j is the mode index; and e is the electron charge.

In the above equations, the rate $\partial N_i/\partial t$ of change in the carrier concentration in the active layer of thickness d_i is determined by the injection current density J_i, the spontaneous recombination of carriers with the characteristic time $\tau_{\rm sp}$, carrier diffusion over the active-region volume with the coefficient D_i and the stimulated recombination of carriers, which is represented by two last terms of the equation. The first term corresponds to the longitudinal S mode and the second term – to the L mode. The dependences of J_i and N_i in (6) on coordinates ρ,φ and time are omitted for brevity and the parameter

$$\Gamma_i^{\rm L/S} = \frac{d_i^{-1}\int_{d_i}|f(z)|^2{\rm d}z}{L_{\rm cav}^{-1}\int_{L_{\rm cav}}|f(z)|^2{\rm d}z} \tag{7}$$

is introduced, which is usually called the gain-enhancement factor [13]. Equation (6) is written in the form averaged along the z axis and the above coefficient shows how much the photon density averaged over z in the ith active region of thickness d_i differs from the photon density averaged over the entire cavity of length $L_{\rm cav}$.

The rate equations for the photon density in modes are written in the form:

$$\frac{\partial S^{{\rm L/S},j}}{\partial t} = G^{{\rm L/S},j}S^{{\rm L/S},j} + \frac{\eta}{\tau_{\rm sp}}\left\langle N_1^{{\rm L/S},j}\right\rangle_{\rm act} + \frac{\eta}{\tau_{\rm sp}}\left\langle N_2^{{\rm L/S},j}\right\rangle_{\rm act}. \tag{8}$$

Here, the relation of the rate $\partial S^{{\rm L/S},j}/\partial t$ of change in the photon density in the jth transverse mode with the mode gain $G^{{\rm L/S},j}$ is written and the contribution of the fraction η of photons generated due to spontaneous carrier recombination in both cavities is taken into account. The mode gain is represented in the optical part of the model as $G^{{\rm L/S},j} = -2\,{\rm Im}(\omega^{{\rm L/S},j})$. The value of $\left\langle N_i^{{\rm L/S},j}\right\rangle_{\rm act}$ is the carrier concentration averaged by the volume of the ith active region and the mode profile. The mode profiles are assumed normalised as

$$\frac{1}{L_{\rm cav}}\int_{L_{\rm cav}}|f(z)|^2{\rm d}z = 1;\ \ \frac{1}{\pi R_{\rm act}^2}\int_{s_{\rm act}}\left|\Phi^{{\rm L/S},j}(\rho,\varphi)\right|^2{\rm d}\rho{\rm d}\varphi = 1.$$

The output power of the laser is calculated as follows.

The total output power of the CC-VCSEL transverse mode can be found from simplest reasons as the ratio of the number of coherent photons in this $SV_{\rm cav}$ mode multiplied by the energy of one photon and divided by the photon lifetime $\tau_{\rm ph}$ in the 'cold' cavity:

$$P_{\rm out} = \frac{\hbar\omega SV_{\rm cav}}{\tau_{\rm ph}},$$

where $V_{\rm cav}$ is the cavity volume.

The photon lifetime in the cavity is determined as the value inverse to the mode decay in the 'cold' cavity.

On the other hand, the output power can be estimated by knowing the photon density of the mode at the output mirror:

$$P_{\rm out} = \hbar\omega\frac{c}{n_{\rm g}}S\pi R_{\rm act}^2\left\langle|f(z)|^2\right\rangle_{\rm out}.$$

In the structure under study we used isolating apertures of small diameter providing single-mode generation both in the theory and experiment. Therefore, the total output power in each of the longitudinal modes could be set equal to the power of the fundamental transverse mode.

Table 1. Parameters of CC-VCSEL layers.

Layer	Material	Thickness/nm	Refractive index
Air	Air	∞	1
Top BM, 24 pairs of layers	$GaAs/Al_{0.9}Ga_{0.1}As$	66.7/76.3	3.53/3.08
Cavity 1 (top)	$Al_{0.15}Ga_{0.85}As$	265.4	3.40
four InGaAs quantum wells	InGaAs	8	3.60
Isolating aperture	AlAs	15.3	2.95 ($\rho < R_{act}$)
	Al_2O_3		1.60 ($\rho > R_{act}$)
Middle BM, 8.5 pairs of layers	$GaAs/Al_{0.9}Ga_{0.1}As$	66.7/76.3	3.53/3.08
Isolating aperture	AlAs	15.3	2.95 ($\rho < R_{act}$)
	Al_2O_3		1.60 ($\rho > R_{act}$)
Cavity 2 (bottom)	$Al_{0.15}Ga_{0.85}As$	287.5	3.40
two InGaAs quantum wells	InGaAs	8	3.60
Bottom BM, 25 pairs of layers	$GaAs/Al_{0.9}Ga_{0.1}As$	66.7/76.3	3.53/3.08
Substrate	GaAs	300000	3.53
Air	Air	∞	1

3. Parameters of the laser

In this paper we study numerically a CC-VCSEL whose parameters are presented in Table 1 and correspond to the parameters of lasers investigated experimentally in [2, 4, 7].

The laser is formed by two cavities coupled through the middle Bragg mirror. Laser mirrors were made of the GaAs/$Al_{0.9}Ga_{0.1}As$ layers deposited on a substrate and the Bragg wavelength for them was 940 nm. The top, middle and bottom mirrors have 24, 8.5 and 25 pairs of layers and the reflection coefficients at the Bragg wavelength calculated by the matrix method [14] were 99.8 %, 69.3 % and 99.6 %, respectively. The radiation is coupled out through the substrate.

The CC-VCSEL has two isolating oxide apertures of radius 5 μm, which provide optical confinement of the radiation field and specify the area of each of the active regions by spatial confinement of the injection current. Active layers in the cavities have two and four InGaAs quantum wells. The parameters of the active layers are presented below.

Parameters of the CC-VCSEL active region

Spontaneous recombination time τ_{sp}/s ..... 10^{-9}
Ambipolar diffusion coefficient $D_i/cm^2\ s^{-1}$ 1
Spontaneous emission factor η/s ..... 2.6×10^{-4}
Nonlinear refraction coefficient $\frac{dn}{dN}/cm^3$ ..... -6.9×10^{-21}
Carrier concentration for the transparency N_{trans}/cm^{-3} ..... 1.8×10^{18}
Gain g_0 for λ^S/cm^{-1} 1800
Gain g_0 for λ^L/cm^{-1} 2000

4. Results

4.1 General features of CC-VCSELs

The key feature of a CC-VCSEL is the splitting of the longitudinal mode, which falls into the gain profile, into two modes due to the interaction of the fields in the cavities. The spectral interval between these modes and the intensity distribution inside the device are determined by the laser design and, in the first place, by the strength of coupling between the cavities and the ratio of their optical lengths (Fig. 2).

In the case when the laser cavities are of the same optical length, the intensity distributions of the longitudinal modes almost coincide and strongly overlap. This leads to a significant spatial competition of generated modes upon burning out the inverse population in the active layers. According to the performed calculations, in this construction the longitudinal mode, which has a higher gain, will achieve first the lasing threshold and because of burning out the carriers in both cavities will not allow the second longitudinal mode to achieve the lasing threshold. One can avoid this effect by detuning resonators, which makes several percent of their optical length. In such a structure longitudinal modes are localised in their own cavities and stable two-frequency lasing appears. The mode intensity distribution with a longer wavelength is concentrated in longer cavities and the mode intensity distribution with a shorter wavelength – in shorter cavities. The value of detuning also determines the spectral interval between longitudinal modes – the higher is this value and the weaker is the coupling between cavities, the stronger the modes split. For example, when the detuning between cavities was 4 % and the reflection coefficient of the middle mirror at the Bragg wavelength was 69.3 %, the spectral interval between modes was 26 nm. Thus, the degree of longitudinal mode overlapping determining the possibility of two-frequency

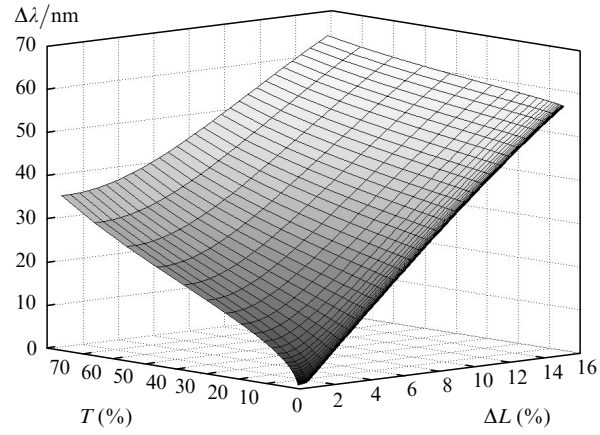

Figure 2. Dependence of the spectral interval $\Delta\lambda$ between the modes on the transmission coefficient T of the middle BM and detuning ΔL between the cavities.

lasing is directly related to the spectral interval between L and S modes: the more is the frequency difference, the weaker is the mode overlapping.

In practice because of inaccuracies of device fabrication, temperature effects, noise oscillations of the carrier concentration and other factors, the real optical lengths of cavities differ even if the cavities themselves were assumed equal.

A detailed study of different variants of the CC-VCSEL mode structure with the use of the optical part of this model can be found in [15].

4.2 Mode structure

Figure 3 shows the intensity distribution of the longitudinal mode of the laser under study. One can see that the mode overlapping with the active layers of the 'foreign' cavity is not too high. This allows one to realise the two-frequency lasing regime. The values of the mode gain-enhancement factors calculated by (7) can serve as a quantitative estimate: $\Gamma_1^S = 8.87$, $\Gamma_2^S = 2.49$, $\Gamma_1^L = 2.13$, $\Gamma_2^L = 10.61$. The presented values represent the ratios of the intensities in active regions to the average value of the intensity in the entire cavity. The reason for difference in coefficients $\Gamma_i^{L/S}$ is the different number of quantum wells in active regions and the asymmetry of longitudinal mode distribution of the laser.

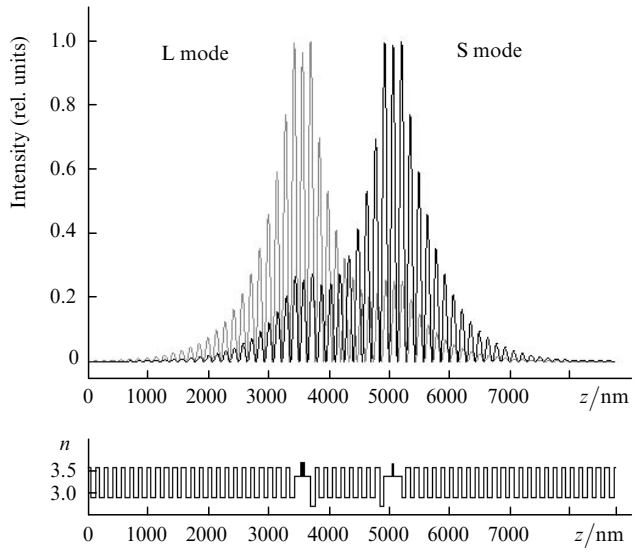

Figure 3. Intensity distribution of longitudinal modes of the CC-VCSEL under study.

In our calculations and in experiments [2, 4, 7], single-transverse mode lasing of LP_{01} modes was observed in both cavities, which is explained by a small diameter of isolating apertures. The intensity distribution of CC-VCSEL transverse modes does not differ substantially from similar distributions, which are well described by the Bessel functions [9] in conventional VCSELs. The profiles of transverse modes of one order, in our case corresponding to different longitudinal modes, slightly differ from each other. This feature is related to the fact that its own cross-section profile of the effective refractive index, which determines the shape of transverse mode, corresponds to each longitudinal mode.

4.3 Lasing dynamics

Figure 4 presents an example of a transient process in CC-VCSELs calculated under the conditions of excitation of two longitudinal modes. The shape of the time dependences for the photon concentration in modes is related to the cross burning out of carriers in the cavities.

Of special interest is the problem of determining the threshold currents in CC-VCSELs. Unlike conventional lasers, in the case under study it is necessary to investigate not single values of threshold currents but curves representing a set of pairs of injection current values. These curves (both calculated and experimental) are presented in Fig. 5. The boundaries of the emission spectrum of CC-VCSELs were obtained by calculating the transient processes similar to the process in Fig. 4 for the corresponding pairs of the

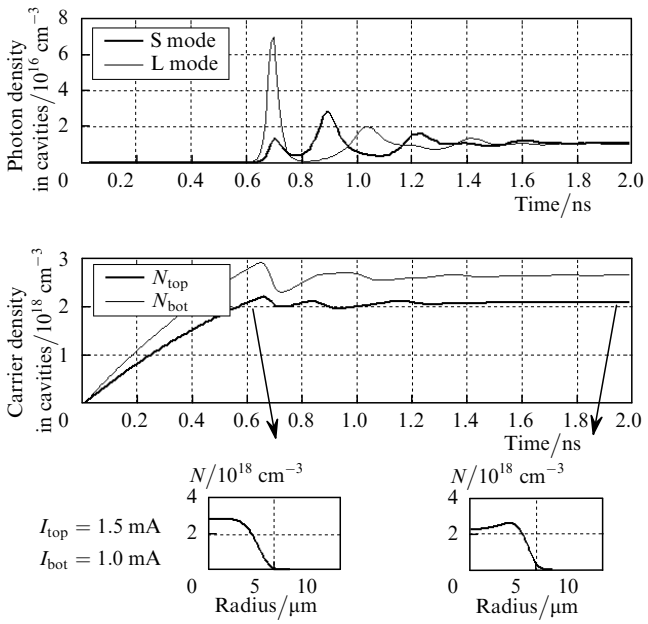

Figure 4. Example of a transient process in the CC-VCSEL; N_{top}, N_{bot} and I_{top}, I_{bot} are carrier densities and currents in the top and bottom cavities, respectively.

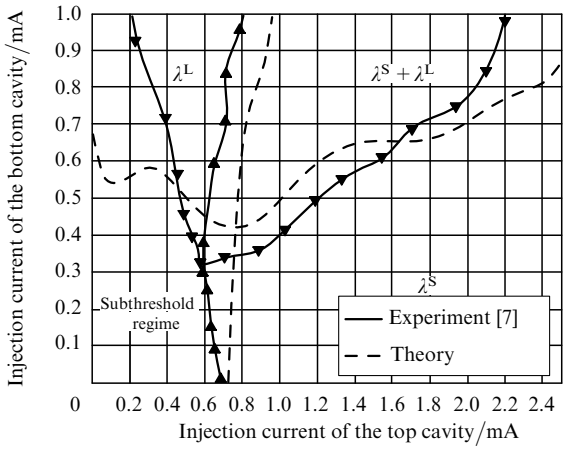

Figure 5. Threshold current curves in CC-VCSELs (experimental data are borrowed from [7]).

injection currents. After this, the curves of the threshold currents were approximated by the polynomials of different degrees.

The plot presented in Fig. 5 can be used to determine the working emission spectrum of CC-VCSELs. Thus, two-frequency lasing starts at the values of the injection currents of the bottom and top cavities $I_{bot} = 0.32$ mA, $I_{top} = 0.60$ mA in the experiment and $I_{bot} = 0.42$ mA, $I_{top} = 0.75$ mA in the theory. This point can be called the threshold of two-frequency lasing of the laser under study, which is analogous to the lasing threshold of a conventional laser. To excite simultaneously the generation of two modes, it is in principle necessary to pump both active regions or to provide optical pumping of the second cavity by the radiation from the first cavity.

The shape of plots in Fig. 5 is common for CC-VCSELs of different designs. Its qualitative character can be explained as follows. In the limiting case, if the CC-VCSEL cavities are not coupled with each other, we should consider two separate VCSELs having the threshold currents which are independent of the injection current of the other laser. In this case the plot in Fig. 5 would look like intersecting vertical and horizontal straight lines. However, in a real device CC-VCSEL cavities are coupled with each other. As was stated above, the main mechanisms, which couple their active regions, are resonance photon absorption in the underexcited cavity and competition of longitudinal modes during burning out the inversion in both cavities. These are these processes which determine the presence of the slope in the presented curves.

Indeed, quantum wells, which do not have enough carrier concentration to produce inverse population, are absorbers. This results in an increase in the values of threshold currents in the laser, where only one cavity is pumped. In the experiment this effect was clearly observed: in CC-VCSELs in the absence of pumping in the top cavity (see Fig. 5), generation localised in the bottom cavity of the L mode does not occur. In calculations this effect is manifested in the increase in the excitation threshold of the L mode. This discrepancy, in our opinion, is related to the approximate character of the dependence of the gain on the carrier concentration (5) and incomplete coincidence of the calculated parameters of the device with the parameters of a real device.

Therefore, in the case when the pumping of one of the cavities is insufficient to generate a mode localised in it, the further increase in pumping will decrease the threshold current of the mode localised in the other cavity.

If the pumping of one of the cavities is sufficient to generate the mode localised in it, mode competition appears in the laser and the situation changes the other way round. The influence of the longitudinal mode competition on the shape of threshold curves is easily observed if the pumping of one of the cavities is constant and the current of the other is increased. The increase in the cavity pumping will lead to an increase in the photon density of the mode corresponding to it. This, in turn, will increase the stimulated recombination rate in active regions due to an increase in the intensity of the standing wave in the cavity. The gain in the cavity with the constant current will start decreasing because the burning out of the carriers in it increases while their income does not increase. As a result, the conditions for mode generation localised in this cavity stop fulfilling. One can see it in Fig. 5: as the pumping of the top cavity increases, the region of injection currents for which generation of L mode localised in the bottom cavity takes place, starts narrowing down despite the fact that the summed injection current of the cavities increases.

The same effect can be observed when considering light–current parameters of the laser (Fig. 6). As the injection current of the top cavity increases, the power of the L mode increases, achieves maximum (corresponding to the threshold point of the S mode with $I_{top} = 0.7$ mA) and vanishes at $I_{top} = 1.2$ mA. Note that with this current the light–current characteristics of the S mode show a small kink related to the switching off of the L mode.

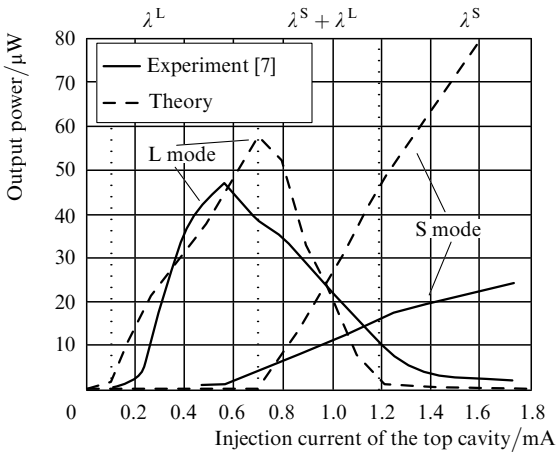

Figure 6. Light–current characteristic of the CC-VCSEL, the injection current of the bottom cavity is $I_{bot} = 0.6$ mA (experimental data are borrowed from [7]).

Therefore, in the case when the pumping of one of the cavities is sufficient to generate the mode localised in it, a further increase will result in the increase in the threshold current of the mode localised in the other cavity.

Note also the following peculiarity of CC-VCSELs. On the light–current characteristics at the point corresponding to the injection current $I_{top} = 1$ mA, both modes have nearly the same power, however, the photon densities in them differ by five. This is explained by the fact that the mode localised in the cavity nearest to the output mirror has the optimal condition for coupling out radiation. The mode localised in the farther cavity will be separated from the output not by one but two Bragg mirrors, due to which the main part of its power will be coupled out into the other side. One should take this into account during the fabrication of CC-VCSELs. If the reflection coefficient of the middle mirror is too high, the difference between powers of modes can prove too large for practical applications of two-frequency lasing.

One can see from the comparison of the results that our model agrees well with the experiment and allows one to explain the main mechanisms in the operation of CC-VCSELs. The discrepancies between the theoretical and experimental data in many cases do not exceed 15 % – 20 % from their values, which substantially improves the simulation accuracy achieved in paper [7]. The discrepancy between the measured and calculated light–current parameters for the S mode are slightly higher of this value. In our opinion this is explained by the presence of resonance effects in the substrate through which the radiation is coupled out.

These phenomena are difficult to take into account without the accurate data on the thickness of the substrate and the presence of an antireflection coating on the emitting surface.

The further development of this work can involve the consideration of the temperature features of the device operation and the study of such phenomena as self-modulation and optical bistability in CC-VCSELs.

Thus, a self-consistent dynamic model of a coupled-cavity vertical-cavity surface-emitting laser has been realised. The model allows the calculation of the frequency of the generated mode of the laser together with the gains, threshold current curves, which determine the regions of two-mode and single-mode generation, light – current characteristics of the device and the study of transient processes in the CC-VCSEL. The obtained data are in good agreement with the experiment described in paper [7].

References

1. Iga K. *IEEE J. Sel. Top. Quantum Electron.*, **6**, 1201 (2000).
2. Brunner M., Gulden K., Hovel R., Moser M., Carlin J.F., Stanley R.P., Ilegems M. *IEEE Photonic. Technol. Lett.*, **12** (10), 1316 (2000).
3. Fischer A.J., Choquette K.D., Chow W.W., Allerman A.A., Serkland D.K., Geib K.M. *Appl. Phys. Lett.*, **79**, 4079 (2001).
4. Badilita V., Carlin J.-F., Ilegems M., Brunner M., Verschaffelt G., Panajotov K. *IEEE Photonic. Technol. Lett.*, **16**, 365 (2004).
5. Carlin J.-F., Stanley R.P., Pellandini P., Oesterle U., Ilegems M. *Appl. Phys. Lett.*, **75**, 908 (2000).
6. Fischer A.J., Choquette K.D., Chow W.W., Allerman A.A., Geib K.M. *Appl. Phys. Lett.*, **77**, 3319 (2000).
7. Badilita V., Carlin J.-F., Ilegems M. *IEEE J. Quantum Electron.*, **40** (12), 1646 (2004).
8. Coldren L.A., Ebeling K.J., Rentschier J.A., Burrus C.A., Wilt D.P. *Appl. Phys. Lett.*, **44** (4), 368 (1984).
9. Yu S.F. *Design and Analysis of Vertical Cavity Surface Emitting Lasers* (New York: Wiley & Son, 2003).
10. Wenzel H., Wunsche H.J. *IEEE J. Quantum Electron.*, **33**, 1156 (1997).
11. Smolyakov G.A., Osinski M. *IEEE J. Light. Techn.*, **23** (12), 4278 (2005).
12. Bienstman P., Baets R., Vukusic J., et al. *IEEE J. Quantum Electron.*, **37** (12), 1618 (2001).
13. Mulet J., Balle S. *Phys. Rev. A*, **66**, 053802 (2002).
14. Li H., Iga K. (Eds) *Vertical-Cavity Surface-Emitting Laser Devices* (New York: Springer, 2002).
15. Logginov A.S., Rzhanov A.G., Skorov D.V. *Kvantovaya Elektron.*, **36** (6), 520 (2006) [*Quantum Electron.*, **36** (6), 520 (2006)].